Bioinformatics, 37(24), 2021, 4851–4856
doi: 10.1093/bioinformatics/btab557
Advance Access Publication Date: 30 July 2021
Original Paper

OXFORD

Bioimage informatics

spheresDT/Mpacts-PiCS: cell tracking and shape retrieval in membrane-labeled embryos

Wim Thiels [1], Bart Smeets [2], Maxim Cuvelier [2], Francesca Caroti [1] and Rob Jelier [1,*]

[1]CMPG, M2S Department, KU Leuven, Heverlee 3001, Belgium and [2]MeBios, Department of Biosystems, KU Leuven, Heverlee 3001, Belgium

*To whom correspondence should be addressed.

Associate Editor: Jinbo Xu

Received on March 1, 2021; revised on July 16, 2021; accepted on July 28, 2021

Abstract

Motivation: Uncovering the cellular and mechanical processes that drive embryo formation requires an accurate read out of cell geometries over time. However, automated extraction of 3D cell shapes from time-lapse microscopy remains challenging, especially when only membranes are labeled.

Results: We present an image analysis framework for automated tracking and three-dimensional cell segmentation in confocal time lapses. A sphere clustering approach allows for local thresholding and application of logical rules to facilitate tracking and unseeded segmentation of variable cell shapes. Next, the segmentation is refined by a discrete element method simulation where cell shapes are constrained by a biomechanical cell shape model. We apply the framework on *Caenorhabditis elegans* embryos in various stages of early development and analyze the geometry of the 7- and 8-cell stage embryo, looking at volume, contact area and shape over time.

Availability and implementation: The Python code for the algorithm and for measuring performance, along with all data needed to recreate the results is freely available at 10.5281/zenodo.5108416 and 10.5281/zenodo.4540092. The most recent version of the software is maintained at https://bitbucket.org/pgmsembryogenesis/sdt-pics.

Contact: rob.jelier@kuleuven.be

Supplementary information: Supplementary data are available at *Bioinformatics* online.

1 Introduction

Modern fluorescence microscopy allows for the detailed imaging of all cells in a multi-cellular system over time. Following cells and their shapes can provide information about cellular mechanics, cell–cell interactions and force generation, which are constituents of the processes that underlie cellular self-organization (Keller, 2013). However, automated 3D cell shape reconstruction from microscopy of multi-cellular systems with labeled membranes remains challenging in practice. In this article, we develop an innovative method to accurately segment cells and retrieve 3D meshes using the *Caenorhabditis elegans* embryo as a model.

There are several issues that complicate working with this type of data. Phototoxicity places biological constraints on the signal strength especially during time lapses, while photobleaching and light scattering deeper in the sample typically leads to a degradation of signal quality over time and depth. The problem is compounded by the relatively limited z-resolution in standard confocal and wide-field microscopy. Furthermore, some systems, such as early embryo development, feature cells with variable and changing cell shapes and sizes.

Various techniques have been used in current cell segmentation pipelines (Meijering, 2012), including deformable models such as level sets (Grushnikov *et al.*, 2018; Uba *et al.*, 2020) and active meshes (Dufour *et al.*, 2011) along with machine learning approaches, such as pixel classification methods (Hilsenbeck *et al.*, 2017) and convolutional neural networks (Cao *et al.*, 2020; Supplementary Table S5), though the most widely used technique appears to still be the watershed algorithm (Beucher, 1990; Stegmaier *et al.*, 2016; Supplementary Table S5).

The effectiveness of a given technique strongly depends on the way both over-segmentation and gap sensitivity are handled. Over-segmentation can occur due to signal noise, apparent membrane signal inside cells or irregular cell shapes, amongst other reasons. The issue can be dealt with procedurally, e.g. by a clustering approach in the case of watershed regions (Beucher and Marcotegui, 2009), but more commonly the problem is addressed by providing the algorithm with seeds marking the cells, either by manual annotation or by adding a nucleus channel (Amat *et al.*, 2014; Azuma and Onami, 2017; Cao *et al.*, 2019; Machado *et al.*, 2019). The latter has the drawback that an extra marker channel needs to be used. This produces extra technical overhead during imaging, and more crucially

limits how many other markers can be imaged in the experiment, given that the number of fluorescent markers is often limited to two or three in practice. The second challenge is handling gaps in the membrane signal. The gaps can result in segmentation errors where a cell region spills over into extra-cellular space or neighboring cells. Techniques to help close these membrane gaps include morphological operations (Serra and Soille, 1994; Stegmaier *et al.*, 2016), tensor voting (Mosaliganti *et al.*, 2012) and surface regression (Cao *et al.*, 2019). However, these techniques are not sufficient to fully resolve gaps from noisy confocal images, especially when working in 3D, given the sparse z-resolution of the microscopy input data. An advantage of deformable approaches over watershed in this respect is the introduction of shape constraints which better enable them to reconstruct shapes in regions of poor membrane signal. However, using these methods in the context of multi-cellular aggregates often requires complex algorithm adaptations and high computational cost, which explain their limited use in embryo segmentation software (Dufour *et al.*, 2011). Moving from a continuous deformable model to a discrete particle-based simulation can help to overcome these issues, as has been demonstrated by LimeSeg (Machado *et al.*, 2019). Limeseg's approach is similar to a coarse-grained modeling of a lipid membrane where the 'lipid' particles are attracted to high intensity pixels, making it applicable to a broad range of segmentation scenarios, well beyond cell segmentation. However, this broad applicability is reflected in generic shape constraints, and thus can still lead to cell shapes not allowed under the laws of cell mechanics. Overall, the constraints placed on the segmentation by these methods are aimed at reconstructing smooth segmentations, but do not represent well-described properties governing cell shapes, such as cellular adhesion and the mechanical properties of the cellular cortex.

Here, we introduce new methods to robustly identify and track cells in membrane labeled 3D time-lapse images followed by accurate shape retrieval using a biophysical cell shape model. After clarifying the basic design and rationale, we present the tracking and segmentation results obtained on *C.elegans* embryos. Next, we compare our method to RACE, LimeSeg and CShaper. Finally, the software is used to analyze the geometry of the 7- to 8-cell stage.

2 Algorithm

Our design approach is aimed at segmenting and tracking membrane-labeled images of cells with variable shapes, without using additional information to identify the cells. The cell shapes are retrieved in three stages (Fig. 1A). The first stage is an image filter pipeline to identify pixels with membrane signal (Supplementary Material S2, Supplementary Fig. S1). This stage would likely require optimization between microscopy platforms and biological systems. The second stage is a robust and readily optimized algorithm for finding, tracking and roughly segmenting cells, and should be broadly applicable (Supplementary Material S3). The third stage uses a biomechanical model of cell shape to refine the cell segmentations (Supplementary Material S4). A detailed description can be found in Supplementary Information.

2.1 Tracking and coarse segmentation

After membrane localization (Supplementary Material S2), the spheresDT algorithm (Fig. 1B, Supplementary Material S3.1) identifies and tracks the cells, while also providing a coarse 3D cell segmentation. SpheresDT is a progressive clustering algorithm that operates on a 3D distance transform (DT) image stack calculated from the binary membrane images. If the DT-value of a pixel at location (x, y, z) equals r, then one can position a sphere with radius r and center (x, y, z), and by definition, this sphere will take up the maximum of volume without overlapping any membrane pixel. As such, the DT-stack is filled up with spheres in an iterative way, starting with the biggest sphere possible, gradually going down in size until a predefined minimum sphere size is reached. A sphere never overlaps with a membrane pixel, but spheres can mutually overlap leading to the formation of clusters, which in turn get grouped into cells (Supplementary Fig. S2). The cells are subsequently tracked over time by passing on cell labels from one time point to the next and checking for cell divisions at every time step. During clustering, the maximum distance transform value of the overlap zone is used to gauge the size of the membrane gap between the two spheres or clusters, given that this value reflects the radius of the biggest sphere that can be placed inside the overlap zone. This value is compared to a clustering threshold that scales with the radius of the smallest sphere or cluster within the pair. The combined effect is a clustering criterion determined by the size of the membrane gap relative to the size of the smallest object within the pair being considered. In addition, the hierarchy build up during clustering, ranging from spheres to cells, is subjected to logical rules that guide segmentation and tracking (Supplementary Fig. S3). In the Implementation section, we will demonstrate the benefits of these characteristics on segmentation.

2.2 Physically informed cell segmentation

The Mpacts-PiCS algorithm refines spheresDT's output by constraining the cell segmentation through a mechanical model of cell shape. The Deformable Cell Model (DCM) (Odenthal *et al.*, 2013; Smeets *et al.*, 2019), which is based on the Discrete Element Method (DEM), is used to simulate the forces that give rise to cell shapes, such as cortical tension, cytoplasmic pressure and contact forces between cells. These forces act on the nodes of closed triangulated meshes which represent the cells. The model has been used in a variety of contexts such as tissue mechanics (Van Liedekerke *et al.*,

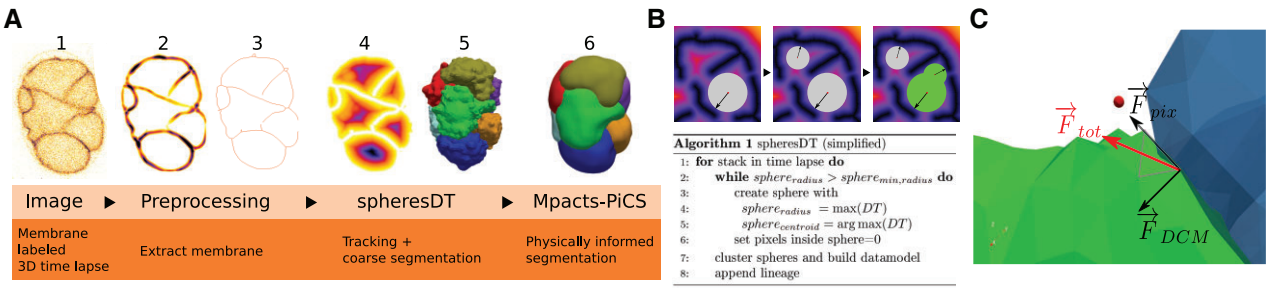

Fig. 1. Design spheresDT/Mpacts-PiCS. (**A**) Overview of the spheresDT/Mpacts-PiCS pipeline. The membrane labeled 3D confocal time-lapse image (1) undergoes preprocessing to identify the membrane. The output of the 2D Frangi filter (2) assigns a vesselness score to each pixel (Supplementary Material S2.1). After a thresholding, size filtering and a thinning operation, a binary membrane image is obtained (3). Next, a sphere clustering algorithm named spheresDT is applied that locates the cells and tracks them over time, reconstructing the lineage tree. The 3D distance transform image (4) derived from the binary membrane is used as input, resulting in coarse cell segmentations where every cell is represented as a cluster of spheres (5). Finally, a segmentation refinement algorithm named Mpacts-PiCS is applied (6). The coarse cell segmentations from spheresDT are inputted into a mechanical simulation whereby the forces that drive cell shape changes are governed by the Deformable Cell Model with an added attractive force originating from the membrane pixels from preprocessing. (**B**) The spheresDT core algorithm. (**C**) Mpacts-PiCS. The force on a mesh node $\vec{F}_{tot}$ that drives the mechanical simulation is composed out of a force resulting from the Deformable Cell Model ($\vec{F}_{DCM}$) and an attractive force from a nearby pixel ($\vec{F}_{pix}$). $\vec{F}_{pix}$ (nN) decreases with distance (μm) according to Equation 12

2020), cell spreading (Odenthal *et al.*, 2013) and contact inhibition of locomotion (Smeets *et al.*, 2016). Image information is introduced into the simulation by inserting membrane pixels into the scenario as an extra attractive force on the cell meshes (Fig. 1C). To calculate forces exerted by the pixels on the cell mesh, the Immersed Boundary Method (IBM) (Guyot *et al.*, 2016) is used.

Utilizing a biomechanical model is a way to use prior knowledge on how cells take their shape and interact with each other in the segmentation. It places mechanical constraints on the segmentation that should ensure physically likely cell shapes. This model driven approach can also help to infer shapes in locations of poor signal quality.

3 Implementation

3.1 A segmentation approach for membrane labeled early-stage embryos

For accurate segmentation of images from membrane labeled early-stage embryos, the method needs to be robust against gaps in the membrane signal as well as avoid over-segmentation. SpheresDT has some unique characteristics, that we demonstrate here using simple segmentation challenges and a comparison to a watershed approach (Fig. 2).

First, to deal with variable cell shapes and sizes one needs to move from a global threshold to a threshold able to vary across space. Such a spatially varying threshold flows naturally from spheresDT given that a different threshold can be set for every pair of overlapping spheres or clusters. The threshold varies in a way that the size of the membrane gap is evaluated relative to the size of the smallest sphere or cluster in the pair. Figure 2A gives an example of a segmentation challenge with several cell shapes. Because watershed uses a global threshold and different cells impose different constraints, it is impossible to find a threshold resulting in correct segmentation. With spheresDT on the other hand, the imposed constraints are compatible, allowing for a correct segmentation. The benefit of using a threshold varying with sphere radius can be seen when looking at cell 1 and cell 2. Both cells have the same shape, but they differ in size, and in spheresDT, these two shapes lead to the same constraint. The need for spatially localized thresholding was also acknowledged in a recent paper (Guignard *et al.*, 2020), where they employ different heuristics based on this concept to improve segmentation and tracking.

Second, spheresDT can limit spillover problems by limiting the resolution of segmentation. Spillover is caused by membrane gaps in the (preprocessed) image that are hard to avoid given the challenging nature of the microscopy data. Figure 2B demonstrates that spheresDT avoids the spillover seen by watershed, by stopping the segmentation process at a certain minimum sphere radius. This is further illustrated in Figure 2C. Combining the minimum sphere radius, which defines the segmentation resolution, with a minimum cell radius allows some flexibility in the segmentation behavior.

Third, spheresDT is embedded in a set of logical rules, not defined at the pixel-level as in most segmentation approaches, but defined on higher level objects represented in the data model that is build up (Supplementary Fig. S2). Figure 2D provides an illustration of such a logical rule involving cell division.

3.2 Lineage reconstruction using only membrane labeling

To demonstrate the accuracy of the spheresDT algorithm, we tracked cells in four developing *C.elegans* embryos. These early-stage embryos, ranging from 2 up to 100 cells, express a fluorescent membrane marker and were recorded for approximately 1 h in 3-min intervals using a confocal microscope. For validation, we compared the automatic lineage reconstruction to manually annotated lineage data. Our evaluation uses the TRA score, together with standard accuracy metrics (Supplementary Material S6.1). The TRA score is a reflection of the effort needed to manually correct the lineage, making it a richer metric compared to sensitivity and precision, which look at each time step separately. SpheresDT achieved an average TRA-score of 0.959, average precision of 0.974 and average sensitivity of 0.943 (Fig. 3A, Supplementary Fig. S15). Only three user parameters needed to be varied across all datasets (Supplementary Table S3): a first parameter controls the sensitivity during the identification of membrane pixels, a second parameter sets the overall clustering threshold and a third parameter defines the minimum cell radius.

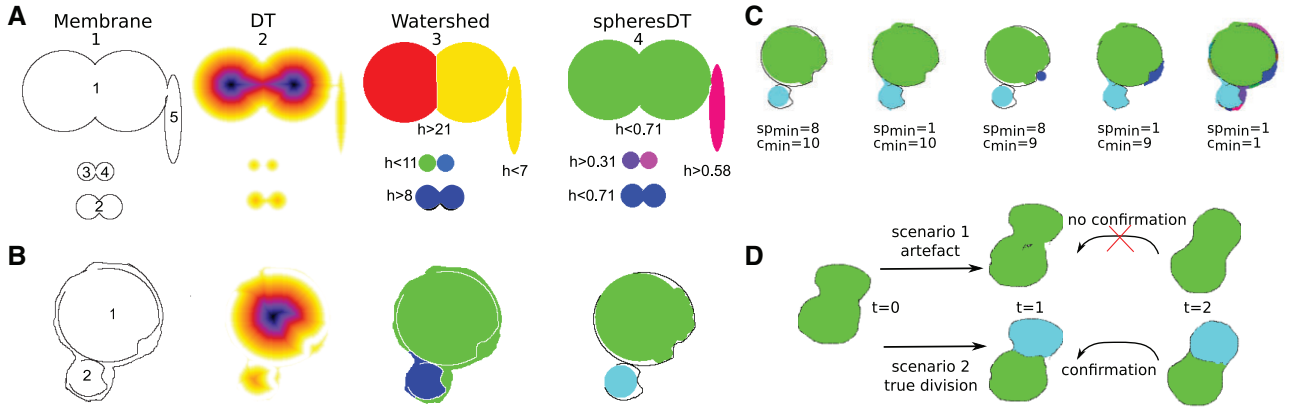

Fig. 2. spheresDT features in comparison to watershed. (**A**) Dealing with varying cell shapes. (1) The ground truth image shows five cells. Cell 1 and 2 have the same shape but cell 2 is smaller. Cell 3 and 4 are small, clearly separate cells with a minor membrane gap in between. Cell 5 has an oblong shape next to cell 1 with a minor membrane gap in between. (2) Distance Transform of the ground truth image. (3) Watershed on the DT-image can never find a threshold (h-maxima transform, Serra and Soille (1994)) leading to a perfect segmentation. (4) Segmentation via spheresDT is able to correctly identify all cells. h corresponds to parameter $fragmentation_{level}$ (Supplementary Material S3.1). Cell 1 and cell 2 will break up in two parts at the same $fragmentation_{level}$ value, because both cells have the same shape, and only differ in size. (**B**) Dealing with membrane gaps. (1) Ground truth image showing two cells with membrane gaps surrounded by an exterior boundary. (3) Watershed on the distance transform allows detecting two cells, but leads to spillover into the exterior. (4) SpheresDT locates both cells without spillover by halting segmentation when the radii of the circles drop below a certain threshold (sp_{min}). A coarser segmentation will be the result. (**C**) spheresDT segmentation allows to control the segmentation by varying the two parameters. sp_{min} controls the resolution of the resulting segmentation, while c_{min} (minimum cell radius) controls the size of the segmentation area that can be detected. A high value of sp_{min} will reduce problems of spillover, but also results in a coarser segmentation. A high value of c_{min} will reduce problems of over-segmentation, but should not be set too high to avoid missing smaller cells. If both parameters are set to the lowest value (one pixel), spheresDT behaves like regular watershed. (**D**) In scenario 1, an image artifact at $t=1$ separates the cell into two different regions. Because this artifact is no longer present at $t=2$, this division will not be confirmed and the cell at $t=1$ will remain unified. On the other hand, in scenario 2 a true cell division occurs and the membrane separating cell 1 from cell 2 will also be present at $t=2$, leading to a confirmation of a cell division at $t=1$

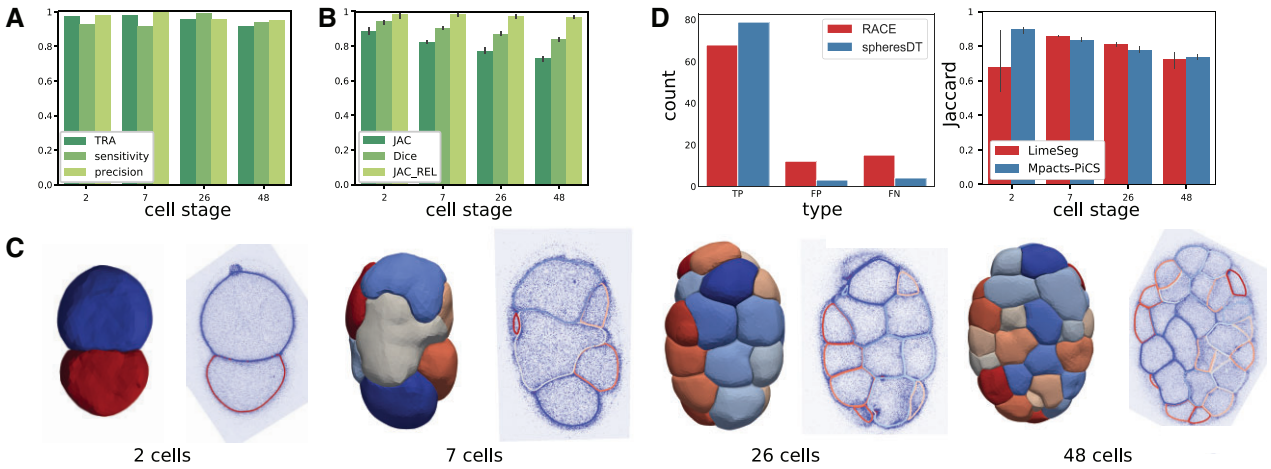

Fig. 3. Results tracking and segmentation. (**A**) Overall tracking scores. Four *C.elegans* embryos were tracked starting from different cell stages using the spheresDT algorithm. Each time step represents an interval of 3 min. TRA evaluates the reconstructed lineage tree as a whole (Supplementary Material S6.1), sensitivity and precision are aggregated measures over all time steps. (**B**) Twelve image stacks representing three replicates of the 2-, 7-, 26- and 48-cell stage were segmented using the spheresDT/Mpacts-PiCS algorithm. Averaged *JAC*, *Dice* and JAC_{REL} scores across the different cell stages are shown. (**C**) Cross-section and 3D segmentation representing the different cell stages. Only the first replicate of the three is shown. (**D**) (left) Cell localization performance of RACE compared to spheresDT. The first time point of the tracking data was used. (right) Comparing segmentation performance of spheresDT/Mpacts-PiCS to LimeSeg. LimeSeg was initialized using manually validated cell centroids

3.3 Physically informed cell segmentation

Twelve image stacks representing three replicates of the 2-, 7-, 26- and 48-cell stage were selected as input. The rough cell outlines determined by spheresDT, parameterized for optimal tracking, were converted into triangulated meshed hulls and used as input for the Mpacts-PiCS algorithm (Supplementary Material S4).

We compared the automatic shape reconstructions produced by Mpacts-PiCS (Supplementary Fig. S16) to manually annotated cell shapes using the Jaccard score (*JAC*) and Dice score (*Dice*), together with a relative Jaccard score (JAC_{REL}) (S6.2). JAC_{REL} is defined as the ratio of the original *JAC* score, with the *JAC* score obtained with manually annotated membrane as pixel input for the mechanical simulation (Supplementary Material S4.4).

Across the 12 embryos, an average *JAC* score of 0.80 was obtained, ranging from 0.71 to 0.90 (Fig. 3B). *JAC* scores tend to decrease with larger cell counts, mainly because the limited z-resolution often causes ambiguity on where one cell ends and another cell begins, and smaller cells have a larger part of their volume affected by these ambiguous slices. Also, with more, and therefore smaller cells, small stretches of membrane missed by membrane extraction can account for a large proportion of a cell's membrane, leading to a big drop in segmentation quality for that cell.

Given that the manually annotated 3D cell shapes themselves are imperfect, especially when the image quality is relatively poor, the JAC_{REL} score was introduced, which scores segmentation relative to a segmentation that uses the manually annotated membrane. This allows to parse out the effect of the membrane extraction on segmentation. JAC_{REL} scores range from 0.96 to 1.01, indicating that membrane extraction (preprocessing) performs close to manually annotated membrane regarding segmentation quality.

For additional validation, we applied our software to the 21 image stacks made available by Cao *et al.* (2020) for which we obtained a precision of 0.87, recall of 0.88 and a DICE score of 0.88 (Supplementary Material S6.5).

3.4 Comparison to RACE, Limeseg and CShaper

Although many segmentation software packages are available, not all are suited for 3D microscopy images with only membrane labeling (Supplementary Table S5). We chose to compare to RACE (Stegmaier *et al.*, 2016), LimeSeg (Machado *et al.*, 2019) and CShaper (Cao *et al.*, 2020).

RACE is state-of-the-art software shown to have excellent performance across different organisms and microscopes and is reported to outperform ACME, EDGE4D and MARS (Stegmaier *et al.*, 2016). We processed the first time point of the aforementioned four time-lapses with RACE and evaluated cell detection performance (Fig. 3D). Parameters were manually set for optimal performance using the first time-lapse to calibrate microscope-related parameters, while data-specific parameters were adjusted for each time-lapse separately (Supplementary Table S6). The results reflect that automated seed detection from RACE underperforms on our data. Next, to bypass the segmentation issues caused by faulty seed detection, we manually provided the seeds to RACE. As Supplementary Figure S20B illustrates, spillover effects are still readily observed across the stacks, especially deeper down the z-stack. Supplementary Figure S21 further demonstrates that one single watershed threshold was not able to give consistent segmentations across the whole stack.

We also compared our segmentation results to LimeSeg, a surfel-based approach which is loosely based on a molecular dynamics simulation of a lipid membrane. Like Mpacts-PiCS it also employs a particle based simulation, but the forces result solely from membrane tensions instead of cell shape mechanics. To initialize LimeSeg, the seeds were manually inputted, and the outward pressure force was adjusted for optimal segmentation. LimeSeg obtained an average *JAC* score of 0.76, compared to 0.8 using our algorithm (Fig. 3D). LimeSeg scores are comparable to Mpacts-PICS, but show a drop in *JAC* score on the 2-cell stage (Supplementary Fig. S22A). Highly irregular surfaces can be outlined by LimeSeg, which amounts to a very flexible approach, but which can also result in unnatural cell shapes in some instances (Supplementary Fig. S22B).

Finally, we compared to CShaper, which uses a convolutional neural network-based approach to identify membrane in the image, followed by a watershed segmentation. Both the pre-trained neural network, and the network trained on our ground truth data did not result in binary membrane images that could be used for further segmentation (Supplementary Material S7.4).

3.5 Geometric analysis of the 7- to 8-cell stage

To demonstrate the practical use of the segmentation approach described earlier, we examined the 7- to 8-cell stage of the *C.elegans* embryo, looking at volume, contact area and sphericity (Supplementary Material S5). Starting from the first time point after EMS division, seven embryos were tracked over 15 min in 3-min intervals (Supplementary Fig. S14).

In line with the literature (Fickentscher and Weiss, 2017; Gönczy and Rose, 2005; Sulston *et al.*, 1983), P2 and EMS were found to divide asymmetrically (Fig. 4A, Supplementary Fig. S7). Contrary to

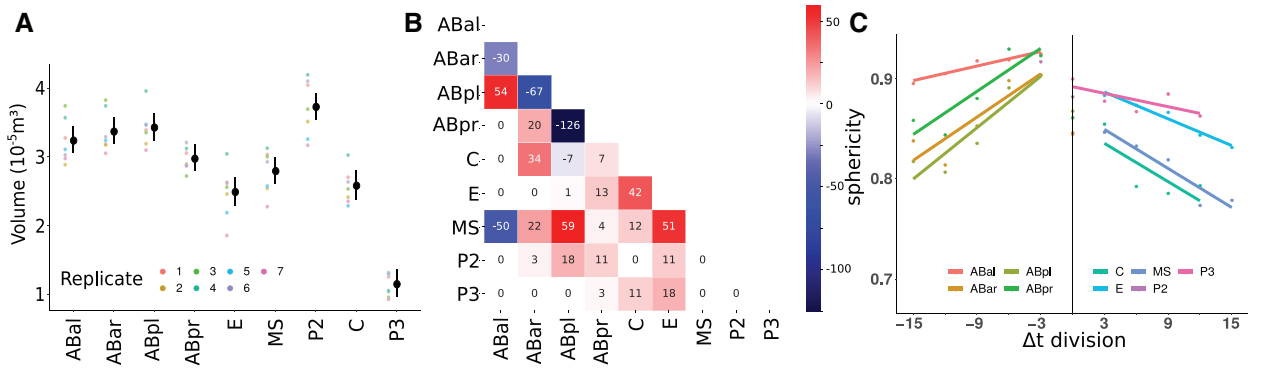

Fig. 4. Analysis of the 7- to 8-cell stage. (**A**) Volume estimates resulting from the mixed model (Supplementary Material S5.1). Black bars indicate the 95% confidence intervals of the volume estimate for each cell type. Note that, because cell size is correlated to the total embryo size, cells with an overlapping confidence interval can be still shown to be significantly different in volume after the correlation to the embryo size is accounted for by the mixed model. EMS division gives rise to a MS daughter cell which is slightly bigger than the E cell (MS/E ratio = 1.12). A noteworthy difference can be seen in the ABpr cell which is significantly smaller (ABpr/ABpl ratio = 0.85) as compared to ABpl and other AB cells. (**B**) Heatmap that shows the change in contact area (in μm^2) between cells between the first and the last appearance of the cell pair in the data (See Supplementary Fig. S11 for more detail). (**C**) Sphericity change over time. The *x*-axis indicates the time to the nearest cell division (3-min intervals). Cells nearing cell division (the AB cells) show consistent rounding. After division, cells lose their sphericity

Fickentscher and Weiss (2017), which states that all AB cells are not significantly different in volume, we found that ABpr is smaller than ABpl, with an estimated ABpr/ABpl ratio of 0.85. To assess the effect of compression during imaging, we performed additional segmentation and subsequent volume measurements based on previously published images (Jankele *et al.*, 2021) for four uncompressed embryos (Supplementary Material S1.1). We found a highly significant effect of compression ($P = 2e\text{-}6$) with an estimated ABpr/ABpl ratio of 0.99 for the uncompressed embryos (Supplementary Fig. S7). To see if this asymmetry can still be detected in later cell stages, we analyzed the volume measurements from Cao *et al.* (2020), which resulted in an ABpr/ABpl ratio of 0.8918, in line with the volume asymmetry we observed in the 7-cell stage (Supplementary Material S5.2).

Next, we tracked the changes in contact area between all nine cells in the 15 min time span (Fig. 4B, Supplementary Material S5.3). Cellular contact area is considered a key determinant of cell communication (Guignard *et al.*, 2020). The most substantial change in contact area reflects the movement of ABpl, where ABpl moves away from ABpr, simultaneously pulling the C cell along (Pohl and Bao, 2010) (Supplementary Figs S13 and S10). Another notable change corresponds to the increase in contact between ABpl and MS during left-right patterning (Pohl and Bao, 2010).

Finally, when tracking sphericity (Fig. 4C, Supplementary Fig. S12), we see the effect of rounding and stiffening of the cells as they approach cell division (Kajita *et al.*, 2002). After cell division, cells tend to lose sphericity and start to spread out (Supplementary Fig. S13). The stretching of C due to the pulling effect of ABpl can also be observed in the sharp decline in sphericity of C.

4 Discussion

With spheresDT/Mpacts-PiCS we offer an approach for cell localization, tracking and 3D segmentation using 3D time-lapse microscopy data with only membrane labeling (Supplementary Material S7.5).

SpheresDT can effectively track cells based on membrane signal alone in a complex 3D environment, as opposed to lineage reconstruction software requiring nuclei staining (Murray *et al.*, 2006). We could achieve high performance for identifying and tracking cells, despite the challenges posed by the dynamic cell shapes in the early *C.elegans* embryo. By employing a spatially varying threshold and coarse segmentation, spheresDT is designed to sidestep the pitfalls of watershed-based approaches such as over-segmentation and spillover, and offers a straightforward way to guide the segmentation process with a limited set of easy to understand parameters. The underlying architecture of spheresDT is generic in nature, making it applicable to different membrane marked datasets and 3D segmentation tasks in general.

With Mpacts-PiCS we advance a novel concept whereby a mechanical simulation evolves 3D cell meshes to achieve precise and physically sound cell reconstructions. Its appeal lies in that it poses 3D constraints arising from internal mechanics, rather than generic smoothness constraints, leading to a scenario in which irregular shapes are only allowed given strong evidence provided by the microscopy image, while unnatural shapes are precluded. It is also useful for cell shape inference in areas of low signal quality, often encountered deeper in the embryo. The Deformable Cell Model includes passive viscoelastic properties of the acto-myosin cortex, which dominate the immediate mechanical response, as well as active traits, such as cortical tension and adhesion forces. Mpacts-PiCS is rooted in the Discrete Element Method, which is an established numerical method with solid foundation in mechanical theory, and which offers many supporting software packages for simulation and visualization. We pose that particle-based simulation can be an effective segmentation strategy, as also demonstrated with LimeSeg.

Applying our method to retrieve detailed 3D cell shape reconstructions from early-stage *C.elegans* embryos, we obtained statistics that highlight the crucial processes relevant for signaling and repositioning of cells in the early embryo, such as asymmetric divisions and cell to cell contacts evolving over time. Asymmetric cell divisions play an important role in embryo development as they underlie axis formation of the body plan and lead to daughter cells with different fates. The differential distribution of cell fate determinants is often accompanied by a difference in volume of the daughter cells. Besides the P0/1/2/3/4 and EMS divisions, all other cell divisions until gastrulation are typically interpreted as being symmetric in volume. However, these assumptions are predominantly extrapolated from 2D segmentations, and few studies have made detailed 3D volumetric measurements across multiple embryos. We could accurately determine the volume asymmetry of the EMS division, which is known to be modest. Surprisingly, we found a significant volume difference between ABpr and ABpl. It is unclear if the asymmetry has biological significance as the cells have equivalent lineage potential (Wood, 1991), though it has been observed that ABpl and ABpr behave differently in the compressed embryo (Jelier *et al.*, 2016; Pohl and Bao, 2010). One possibility is that the volume difference is a consequence of geometric constraints, as the ABp spindle position is oriented by directed cortical flows (Naganathan *et al.*, 2014; Pimpale *et al.*, 2020) that may be affected by the compression of the embryo for imaging, which is supported by our observation that this volume asymmetry disappeared in uncompressed embryos.

Even though this paper's main focus is cell segmentation, it should be viewed as a necessary first step in approaching several interesting biological research questions. The use of a biomechanical

model of cell shape for segmentation opens up a range of options for further analyses of morphology and biomechanics of the developing embryo. Cell shapes can be used to characterize and quantitatively compare cellular morphologies during development, and this type of analysis can highlight differences in behavior across cell types and over time. Likewise, morphological characterization can help identify novel and specific phenotypes during perturbation experiments such as gene knockdowns. Also, the reconstructed 3D cell shapes can be input for inference strategies with the aim of extracting underlying mechanical parameters, for example cortical tensions and adhesions, that support the observed cell geometry. In addition, observing cell shape changes over time can be used to infer the active forces that drive the movements (Brodland *et al.*, 2014; Xu *et al.*, 2018).

Acknowledgement

The authors thank Radek Jankele from the Gönczy Lab (EPFL, Switzerland) for providing the raw images of the uncompressed embryos.

Funding

This work was supported by the Research Foundation—Flanders [11I2921N to W.T., G055017N to R.J., 12Z6118N to B.S., 1S46817N to M.C.]; and KU Leuven [Internal Grant C14/16/060 to R.J.].

Conflict of Interest: none declared.

References

Amat,F. *et al.* (2014) Fast, accurate reconstruction of cell lineages from large-scale fluorescence microscopy data. *Nat. Methods*, **11**, 951–958.

Azuma,Y. and Onami,S. (2017) Biologically constrained optimization based cell membrane segmentation in *C. elegans* embryos. *BMC Bioinformatics*, **18**, 1–11.

Beucher,S. (1990) Segmentation d' images et morphologie mathématique. Ph.D. thesis, École Nationale Supérieure des Mines de Paris.

Beucher,S. and Marcotegui,B. (2009) P algorithm, a dramatic enhancement of the waterfall transformation. École Nationale Supérieure des Mines de Paris. Paris.

Brodland,G.W. *et al.* (2014) CellFIT: a cellular force-inference toolkit using curvilinear cell boundaries. *PLoS One*, **9**, e99116.

Cao,J. *et al.* (2019) 3DMMS: robust 3D membrane morphological segmentation of *C. elegans* embryo. *BMC Bioinformatics*, **20**, 1–13.

Cao,J. *et al.* (2020) Establishment of a morphological atlas of the *Caenorhabditis elegans* embryo using deep-learning-based 4D segmentation. *Nat. Commun*, **11**, 6254.

Dufour,A. *et al.* (2011) 3-D active meshes: fast discrete deformable models for cell tracking in 3-D time-lapse microscopy. *IEEE Trans. Image Process.*, **20**, 1925–1937.

Fickentscher,R. and Weiss,M. (2017) Physical determinants of asymmetric cell divisions in the early development of *Caenorhabditis elegans*. *Sci. Rep.*, **7**, 1–10.

Gönczy,P. and Rose,L.S. (2005) Asymmetric cell division and axis formation in the embryo. *WormBook*, **15**, 1–20.

Grushnikov,A. *et al.* (2018) 3D level set method for blastomere segmentation of preimplantation embryos in fluorescence microscopy images. *Mach. Vis. Appl.*, **29**, 125–134.

Guignard,L. *et al.* (2020) Contact area-dependent cell communication and the morphological invariance of ascidian embryogenesis. *Science*, **369**,

Guyot,Y. *et al.* (2016) Immersed boundary models for quantifying flow-induced mechanical stimuli on stem cells seeded on 3D Scaffolds in perfusion bioreactors. *PLoS Comput. Biol.*, **12**, 1–21.

Hilsenbeck,O. *et al.* (2017) FastER: a User-Friendly tool for ultrafast and robust cell segmentation in large-scale microscopy. *Bioinformatics*, **33**, 2020–2028.

Jankele,R. *et al.* (2021) Physically asymmetric division of the *C. elegans* zygote ensures invariably successful embryogenesis. *Elife*, **10**, 1–66.

Jelier,R. *et al.* (2016) Compensatory cell movements confer robustness to mechanical deformation during embryonic development. *Cell Syst.*, **3**, 160–171.

Kajita,A. *et al.* (2002) Physical effect modeling in of rounding of the *elegans* and cellular stiffening arrangement of the cells embryo. *Genome Inf.*, **13**, 224–232.

Keller,P.J. (2013) Imaging morphogenesis: technological advances and biological insights. *Science*, **340**, 1234168.

Machado,S. *et al.* (2019) LimeSeg: a coarse-grained lipid membrane simulation for 3D image segmentation. *BMC Bioinformatics*, **20**, 2–12.

Meijering,E. (2012) Cell segmentation: 50 Years down the road. *IEEE Signal Process. Mag.*, **29**, 140–145.

Mosaliganti,K.R. *et al.* (2012) ACME: automated cell morphology extractor for comprehensive reconstruction of cell membranes. *PLoS Comput. Biol*, **8**, e1002780.

Murray,J.I. *et al.* (2006) The lineaging of fluorescently-labeled *Caenorhabditis elegans* embryos with StarryNite and AceTree. *Nat. Protoc.*, **1**, 1468–1476.

Naganathan,S.R. *et al.* (2014) Active torque generation by the actomyosin cell cortex drives left-right symmetry breaking. *Elife*, **3**, e04165.

Odenthal,T. *et al.* (2013) Analysis of initial cell spreading using mechanistic contact formulations for a deformable cell model. *PLoS Comput. Biol.*, **9**, e1003267.

Pimpale,L. *et al.* (2020) Cell lineage-dependent chiral actomyosin flows drive cellular rearrangements in early development. *Elife*, **9**, 1–37.

Pohl,C. and Bao,Z. (2010) Chiral forces organize left-right patterning in *C. elegans* by uncoupling midline and anteroposterior axis. *Dev. Cell*, **19**, 402–412.

Serra,J. and Soille,P. (1994) *Mathematical Morphology and Its Applications to Image Processing*, ISMM 2011 edn. Springer, Berlin.

Smeets,B. *et al.* (2016) Emergent structures and dynamics of cell colonies by contact inhibition of locomotion. *Proc. Natl. Acad. Sci. USA*, **113**, 14621–14626.

Smeets,B. *et al.* (2019) The effect of cortical elasticity and active tension on cell adhesion mechanics. *Biophys. J.*, **116**, 930–937.

Stegmaier,J. *et al.* (2016) Real-time three-dimensional cell segmentation in large-scale microscopy data of developing embryos. *Dev. Cell*, **36**, 225–240.

Sulston,J.E. *et al.* (1983) The embryonic cell lineage of the nematode *Caenorhabditis elegans*. *Dev. Biol.*, **100**, 64–119.

Uba,M.K.O. *et al.* (2020) 3D cell image segmentation by modified subjective surface method. *Tatra Mt. Math. Publ.*, **75**, 147–162.

Van Liedekerke, P. *et al.* (2020) A quantitative high-resolution computational mechanics cell model for growing and regenerating tissues. *Biomech. Model Mechanobiol.*, **19**, 189–220.

Wood,W.B. (1991) Evidence from reversal of handedness in *C. elegans* embryos for early cell interactions determining cell fates. *Nature*, **349**, 536–538.

Xu,M. *et al.* (2018) A scheme for 3-dimensional morphological reconstruction and force inference in the early *C. elegans* embryo. *PLoS One*, **13**, 1–20.